Draft Version, 06 July 2026

Enhancing Power System Resilience Under Deep Climate Uncertainty: A Minimax Regret Approach Combined with GNN-cGAN and SWITCH

Jiarui Wang[a], Junqi Liu[b], Lei Zhu[c,*], Gang He[d,e,f,*]

[a] *School of Economics and Management, Beihang University, Beijing, 100191, P. R. China*
[b] *School of Systems Science, Beijing Normal University, Beijing, 100875, P. R. China*
[c] *School of National Safety and Emergency Management, Beijing Normal University, Beijing, 100875, P. R. China*
[d] *Marxe School of Public and International Affairs, Baruch College, City University of New York, NY 10010, USA*
[e] *CUNY Institute for Demographic Research, City University of New York, New York, NY 10010, USA*
[f] *Earth and Environmental Sciences, The Graduate Center, City University of New York, New York, NY 10016, USA*

Abstract

The rising frequency and intensity of extreme weather events introduce deep climate uncertainties that fundamentally challenge the resilience of urban power systems. Conventional deterministic planning approaches are ill-suited to capture such uncertainties, often leading to maladaptive investments and system vulnerabilities. This study develops a data-driven robust planning approach that integrates high-fidelity scenario generation with a two-stage robust optimization framework. We develop a hybrid generative model combining Graph Neural Networks (GNN) and Conditional Generative Adversarial Networks (cGAN) to capture the city's spatiotemporal dependencies in meteorological variables and produce physically consistent, high-resolution climate scenarios. These scenarios are embedded into a two-stage robust planning model based on the Minimax Regret criterion, which identifies resilient investment portfolios adaptable to diverse future climate trajectories. Applied to Lvliang City, China, the results demonstrate that the proposed approach improves system resilience by avoiding investment lock-in and reducing the risk of performance degradation under extreme conditions. Compared to conventional planning methods, the framework achieves a more balanced trade-off between economic efficiency and climate adaptability.

Keywords: Power System Planning; Climate Uncertainty; GNN-cGAN; Minimax Regret; SWITCH Model

1. Introduction

Amidst global efforts to combat climate change and accelerate energy transition, variable renewable energy (VRE), primarily wind and solar, is becoming central to future power systems (Zheng et al., 2025). However, its strong intermittency and weather dependence pose significant challenges to system reliability and economic viability. Traditional capacity expansion planning methods, which rely heavily on deterministic assumptions, are increasingly inadequate under changing climate conditions (He et al., 2016; Alqurashi et al., 2016). As historical data no longer reliably reflects future extremes (Perera et al., 2020), the heightened meteorological sensitivity associated with large-scale integration of VRE has complicated real-time supply-demand balancing (Lund et al., 2015; Impram

*Corresponding Authors.
Email addresses: lions85509050@gmail.com, leizhu@bnu.edu.cn (Lei Zhu), gang.he@baruch.cuny.edu (Gang He)

et al., 2020) and reshaped the planning paradigm (Hirth and Ziegenhagen, 2015; Shair et al., 2021). Specifically, the rising frequency and intensity of compound extreme climate events (Fang et al., 2025) can lead to abrupt output drops and large-scale blackouts (Xu et al., 2025), severely threatening energy system resilience (Panteli et al., 2017; Stürmer et al., 2024). Therefore, endogenously incorporating future climate uncertainty, especially high-impact, low-probability (HILP) extreme weather risks, has emerged as a critical frontier in power system modeling (Bennett et al., 2021; Yang and Wen, 2005; Khodaei et al., 2015; Sinsel et al., 2020).

The vulnerability of highly renewable power systems is magnified during extreme climate events, which often trigger simultaneous disruptions in wind and solar generation while driving spikes in energy demand. This compound shock is most destructive at the city level, where the power grid serves as the backbone for highly interdependent critical infrastructures, including healthcare, communications, and water supply (Kjølle et al., 2012; Nik et al., 2021). Consequently, sudden mismatches in supply-demand driven by climatic factors can easily precipitate system failures and result in socioeconomic losses (Zhuang et al., 2026; Paredes-Vergara et al., 2025; Jasiūnas et al., 2021). To safeguard urban resilience, planning paradigms evolve toward coordinated source-grid-load frameworks that leverage demand-side flexibility to absorb these meteorological shocks (Impram et al., 2020; Denholm and Hand, 2011). Relying on deterministic models leaves urban grids exposed to high-impact extreme events (Ghodeswar et al., 2025), whereas blindly hedging against absolute worst case scenarios yields prohibitive investment premiums that can inadvertently hinder regional decarbonization efforts (Chen et al., 2022). Therefore, developing a robust planning framework that strategically adapts deep climate uncertainty, striking an optimal balance between economic efficiency and resilience to extreme weather events, is urgently required.

To overcome deterministic planning limitations, stochastic programming (SP) and robust optimization (RO) have been widely adopted. For instance, Gu et al. (2026) developed a multistage stochastic framework to minimize expected costs. However, SP often struggles with unprecedented extremes under deep uncertainty (Dupačová, 2002), while traditional RO can be excessively conservative by focusing solely on worst-case scenarios (Yazdani et al., 2023). This paper proposes a data-driven methodology using physically-defined extreme states to identify city level resilient portfolios. Our contributions are twofold: 1) a GNN-cGAN model generating physically consistent climate scenarios that capture compound extremes at city level; and 2) a two-stage Minimax Regret (MMR) model that integrates climate uncertainty into the SWITCH framework via Benders decomposition.

The remainder is structured as follows: Section 2 reviews related work; Section 3 details the assessment framework, covering scenario generation, load forecasting, and the bi-level optimization model; Section 4 applies this framework to Lvliang City's power planning; and Section 5 concludes.

2. Literature Review

Capacity expansion planning models are increasingly inadequate under growing climate uncertainty since they grounded in deterministic assumptions (He et al., 2016; Alqurashi et al., 2016). Heightened meteorological sensitivity with large-scale integration of VRE has complicated real-time supply–demand balancing (Lund et al., 2015; Impram et al., 2020) and reshaped the planning paradigm (Hirth and Ziegenhagen, 2015; Shair et al., 2021). More critically,

climate change amplifies High-Impact, Low-Probability (HILP) events, which can trigger widespread blackouts through concurrent load surges and generation shortfalls (Perera et al., 2020; Panteli et al., 2017; Stürmer et al., 2024). Addressing these challenges requires a transition from capacity-centric optimization toward resilience-oriented planning that explicitly captures deep spatiotemporal uncertainties (Yang and Wen, 2005; Khodaei et al., 2015; Sinsel et al., 2020). Evolving from a passive role, active load-side Demand Response (DR) (Impram et al., 2020) provides flexibility that defers grid investments and mitigates the declining market value of VRE (Konstantelos and Strbac, 2015; Hirth and Ziegenhagen, 2015). This drives a shift toward coordinated source–grid–load planning (Denholm and Hand, 2011), although such frameworks introduce deep spatiotemporal coupling and high computational complexity (Giannelos et al., 2018). Consequently, existing stochastic programming struggles to balance this complexity with adequate tail risk representation, necessitating advanced uncertainty modeling techniques.

With consideration of uncertainties capacity expansion planning models, stochastic Programming (SP) minimizes expected costs through scenario trees (Alqurashi et al., 2016; Khodaei et al., 2015), while Chance-Constrained Programming (CCP) ensures reliability within probabilistic thresholds (Yang and Wen, 2005; Cao et al., 2018). However, both methods are vulnerable under deep uncertainty, they require precise distributions that historical data cannot provide under unprecedented climate extremes, and suffer from exponential scenario growth (Zhao and You, 2021). Robust Optimization (RO) avoids probabilistic assumptions by hedging against worst-case realizations (Conejo and Wu, 2022; Dong et al., 2011), ensuring strict reliability (Gao et al., 2018; Xie et al., 2020) but at the cost of excessive conservatism, often yielding prohibitive investment premiums (Liu et al., 2021). We adopt the MMR criterion, which minimizes the gap between the current and ex-post optimal decisions, thereby guarding against catastrophic losses under extreme scenarios while avoiding the economic inefficiencies inherent to worst-case protection (Jiang et al., 2013). Regardless of the optimization paradigm, decision effectiveness is fundamentally contingent upon the physical fidelity and representativeness of the evaluated uncertainty sets (Wang et al., 2023). Therefore, addressing these modeling challenges necessitates both an advanced optimization criterion and a highly reliable scenario generation method.

In spatiotemporal scenario generation, decision quality fundamentally depends on how well input scenarios capture future uncertainties. While traditional statistical models (e.g., ARMA, Copula) fall short in handling high-dimensional nonlinearities (Chen et al., 2019; Diaz et al., 2016), Generative Adversarial Networks (GANs) have advanced distributional learning (Wang et al., 2025; Morales et al., 2010). Yet, standard GANs often overlook spatial dependencies among distributed resources, risking underestimation of correlated regional failures (Lai et al., 2018). Graph Neural Networks (GNNs) address this by modeling topological correlations in non-Euclidean spaces (Kipf and Welling, 2017), with Spatio-Temporal GNNs further capturing both temporal evolution and spatial dynamics (Yu et al., 2018; Li et al., 2018). Enhanced by Graph Structure Learning, these models can adaptively infer latent dependencies, enabling high-fidelity reproduction of extreme weather patterns without relying on perfect prior topology (Wu et al., 2020; Deng and Hooi, 2021).

Despite notable progress, reliant on deterministic or oversimplified stochastic scenarios cannot adequately capture compound risks from extreme climate events, while optimization paradigms often struggle to reconcile compu-

tational efficiency with solution conservatism, and integrating deep-learning-derived spatiotemporal scenarios into robust planning frameworks remains challenging, hindering the formation of a closed data-driven decision loop. Thus, we propose a data-driven robust planning methodology that fuses GNN-cGAN scenario generation with the MMR criterion to identify resilient, climate-adaptive investment portfolios at city level, which supports resilient city development under extreme climate conditions.

3. Methodology Framework

The proposed framework couples high-fidelity scenario generation with a bi-level robust optimization structure (Fig. 1). Through a decomposition mechanism, it upgrades the SWITCH power system planning model from a deterministic simulator to a stochastic-resilient decision tool, comprising two core modules:

(1) **High-Fidelity Climate Scenario Generation (Input Layer):** This module integrates Graph Neural Networks with Conditional Generative Adversarial Networks to generate physically consistent, high-fidelity climate scenarios. By learning complex spatiotemporal dependencies, it produces diverse scenario sets that serve as boundary inputs for subsequent power system stress testing.

(2) **Minimax Regret-Based Robust Planning (Decision Layer):** A two-stage robust optimization model is developed to manage the trade-off between investment economy and system resilience. In Stage I (Investment), optimal capacity expansion is determined to minimize the maximum regret across the scenario set. Stage II (Operation) then leverages the SWITCH model as a high-resolution operational solver to verify supply-demand feasibility and quantify costs for each climate scenario.

3.1. Data-Driven Uncertainty Modeling

3.1.1. Data-Driven Climate Scenario Generation

To quantify the uncertainty of future meteorological conditions, the proposed scenario generation module generates high-fidelity climate time-series data by learning a generative mapping from historical observations $S_{t-M}, \ldots, S_t$, and conditional cues y (e.g., month, season labels) to future scenarios $S_{t+1}, \ldots, S_{t+H}$ that maximize the conditional likelihood (i.e., $\arg\max \log P(S_{t+1}, \ldots, S_{t+H} \mid S_{t-M}, \ldots, S_t, y)$). This high-dimensional multivariate spatio-temporal modeling challenge is addressed through a data-driven framework combining GNNs and Conditional Generative Adversarial Networks (cGAN). By treating the meteorological vector $S_t \in \mathbb{R}^m$, where m is the number of core meteorological variables, as a graph signal on a dynamic correlation graph, the GNN captures complex multivariate dependencies across both feature and temporal dimensions. The proposed architecture embeds GNNs within the cGAN adversarial framework (Fig. 2) to ensure high-fidelity climate scenario reproduction.

To explicitly capture the intrinsic correlations among multivariate meteorological variables, we abstract the high-dimensional time series as a dynamic correlation graph $\mathcal{G}(t) = (\mathcal{V}, \mathcal{E}, W)$. Moving beyond traditional approaches constrained by predefined static adjacency matrices, we embed Graph Attention Networks (GAT) within both the cGAN's generator and discriminator to dynamically capture latent asymmetric dependencies. Specifically, the

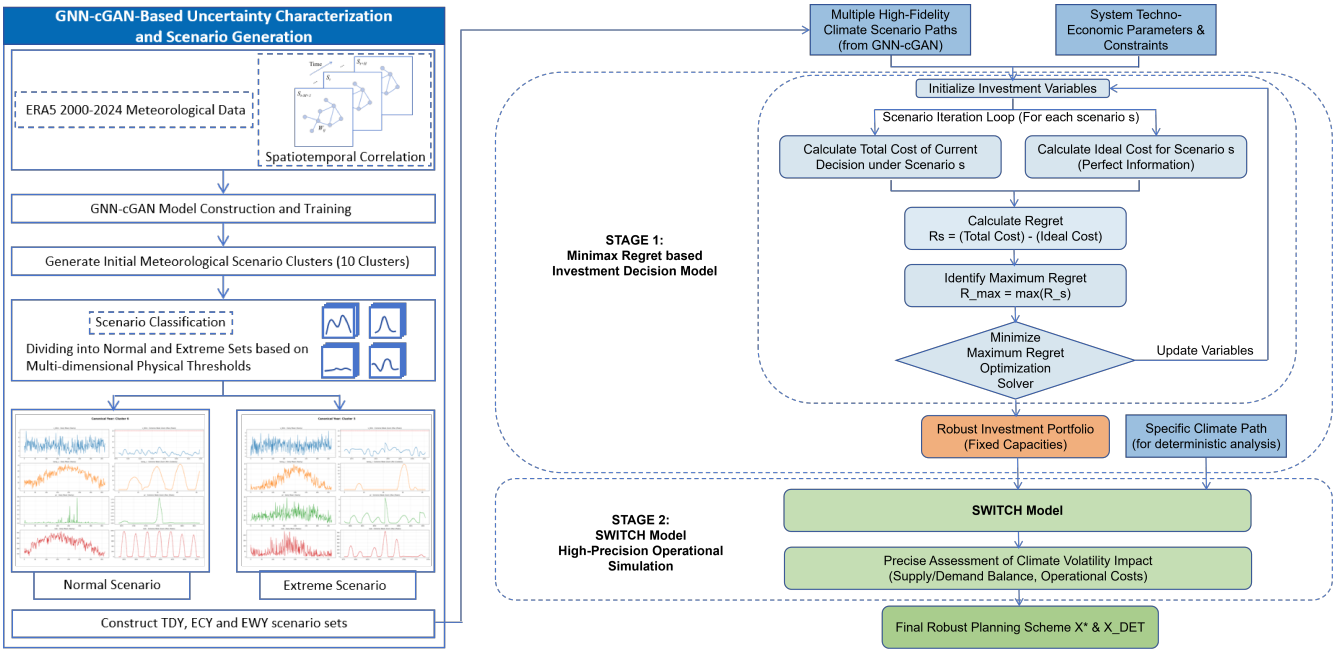

Figure 1: Framework of scenario generation and two-stage robust optimization process.

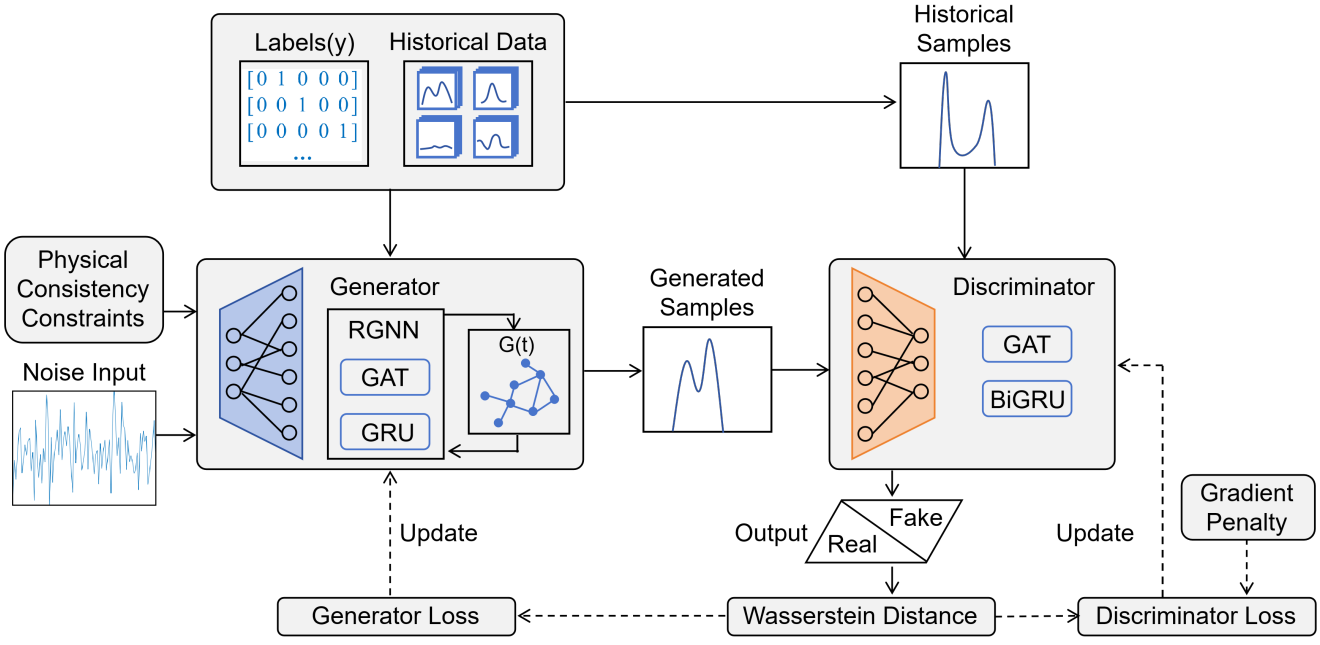

Figure 2: Architecture and training logic of the GNN-cGAN for climate scenario generation.

generator employs a Recurrent Graph Neural Network (RGNN) architecture, integrating GAT with Gated Recurrent Units (GRU) to jointly model spatial multivariate coupling and temporal evolution. To ensure training stability and enforce physical consistency, this adversarial training is optimized using the Wasserstein distance with Gradient Penalty (WGAN-GP) alongside a customized feature matching loss (Qiu et al., 2023). This combination drives the generator to emulate the real meteorological process in both probability density and statistical moments. Complete theoretical and mathematical formulations are detailed in Appendix B.

The GNN-cGAN is trained on ERA5 reanalysis data (2000–2024) (Muñoz Sabater, 2019). The optimized generator is embedded in a Monte Carlo framework to generate 10,000 high-fidelity annual climate scenarios. Compared to limited historical records, this high-density augmentation of the climate distribution effectively mitigates small-sample bias, ensuring the statistical stability and representativeness of the extracted typical and extreme states. This scenario repository supports rigorous post-optimization validation: simulating system operations across diverse meteorological conditions yields reliability metrics, e.g. Loss of Load Probability (LOLP) and Energy Not Served (ENS), to assess whether the planning decisions ensures supply reliability within acceptable bounds. To incorporate these high-dimensional scenarios into a computationally tractable planning framework, the generated data are categorized based on meteorological intensities to construct a discrete scenario tree.

3.1.2. Construction of Climate Scenario Tree and System Inputs

The planning horizon is segmented into year-based intervals with a decision node at each stage. Let N_p denote the total number of decision stages and N_c denote the number of discrete climate states extracted from the generated profiles at each stage (e.g., Typical Data Year (TDY), Extremely Warm Year (EWY), and Extremely Cold Year (ECY) based on Perera et al. (Perera et al., 2020)). As illustrated in Fig. 3, this yields a multi-stage scenario tree rooted in a baseline, generating $(N_c)^{N_p}$ distinct pathways that span stable typical conditions to sequences of persistent extremes. The resulting scenario structure ensures that both typical patterns and extreme climate events are systematically incorporated into the optimization, providing a rigorous stress-test for the subsequent Minimax Regret optimization. Temperature extremes are selected as the primary benchmarks for identifying extreme states due to their dominance over urban load surges, while the GNN-cGAN captures the physically coupled variations in wind and solar potential under these stress conditions.

Once the scenario tree is established, the meteorological conditions of each discrete pathway must be translated into boundary parameters for the power system optimization. To operationalize this, we quantify the impact of generated meteorological scenarios on two critical system inputs, electric load and renewable generation potential. To ensure physical consistency under extreme climate conditions, hourly load is predicted using a pure weather-driven deep learning model (Bi-LSTM) that relies solely on meteorological variables, independent of historical load features. Wind and solar capacity factors are derived from physical models applied to the same meteorological outputs. This phase yields core inputs for the subsequent SWITCH optimization model. Detailed methodology, including model architecture and physical formulations, is provided in Appendix C.

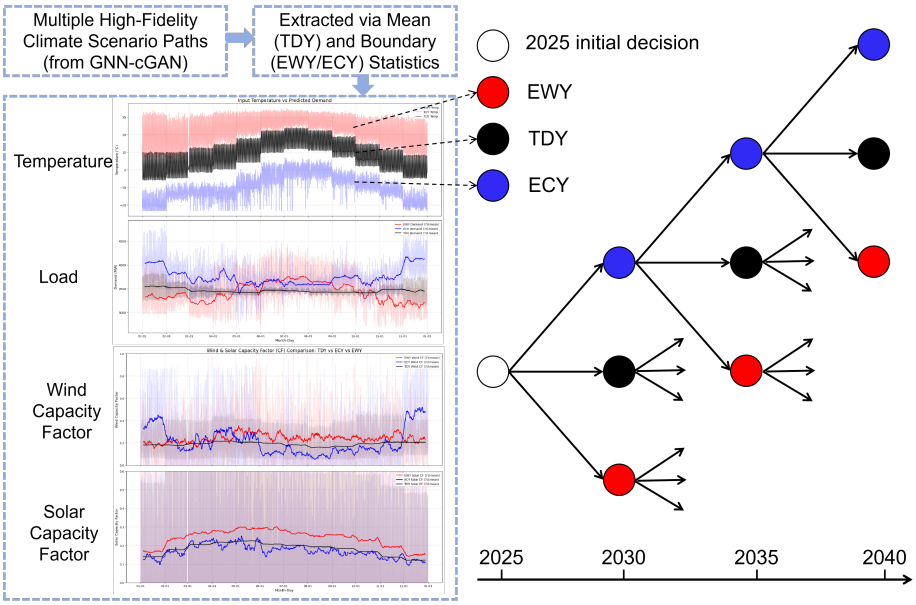

Figure 3: Data-driven spatiotemporal uncertainty modeling framework

3.2. Two-Stage Robust Planning Model

We formulate the generation capacity expansion problem under deep climate uncertainty as a two-stage robust planning model based on the Minimax Regret (MMR) criterion. The goal is to identify an initial investment strategy that minimizes the maximum regret across all potential climate pathways within the constructed scenario tree. Regret represents the opportunity loss: the gap between the total system cost of the adopted plan under a specific uncertainty realization, and the cost of the ex-post optimal plan (e.g. the plan that would have been selected had that realization been known beforehand). By optimizing this metric, the model balances the economic efficiency of the base plan with its adaptability to extreme climate events. The formal mathematical structure is defined as follows:

$$\min_{X\in\chi} \quad \max_{s\in\Omega} \quad \{C_{total,s}(X) - B_s^*\} \tag{1}$$

$$\text{s.t.} \quad X \in \chi := \{0 \le x_{i,p} \le x_{i,p}^{max}, \sum_{i,p} \varepsilon \cdot x_{i,p} \le E_{carbon}^{limit}\} \tag{2}$$

$$Y(X,s) \neq \emptyset, \quad \forall s \in \Omega \tag{3}$$

where the total system cost $C_{total,s}(X)$ under scenario s is determined by the coupling of investment and operational decisions:

$$C_{total,s}(X) = \sum_{p\in P} w_p \left(\sum_{i\in I} c_{i,p} \cdot x_{i,p} + Q_{s,p}(X_p) \right) \tag{4}$$

The second-stage operational cost $Q_{s,p}(X_p)$ represents the minimum system operation cost under a specific

climate trajectory s, formulated as a sub-optimization problem:

$$Q_{s,p}(X_p) = \min_{y_s \in Y(X,s)} \quad \sum_{t \in T_p} (C_{fuel} \cdot P_{s,t} + C_{VOM} \cdot P_{s,t} + VOLL \cdot \Delta P_{s,t}) \tag{5}$$

$$\text{s.t.} \quad \Delta P_{s,t} \geq demand_{s,t} - \sum P_{s,t}, \quad \Delta P_{s,t} \geq 0 \tag{6}$$

In this formulation, B_s^* is a constant parameter representing the optimal baseline cost for scenario s under perfect information, pre-calculated as:

$$B_s^* = \min_{X, y_s} \{C_{inv}(X) + f_{op}(X, y_s) \mid X \in \chi, y_s \in Y(X, s)\} \tag{7}$$

where Equation (1) minimizes the maximum regret cost to ensure that the investment decision remains robust against distributional ambiguity. Constraint (2) defines the feasible investment space by incorporating physical capacity limits and carbon emission caps. Constraint (3) guarantees the existence of a feasible dispatch solution for every scenario s in the uncertainty set Ω, thereby ensuring system reliability under diverse meteorological patterns. This nested optimization framework identifies a resilient investment portfolio X that avoids both excessive conservatism and catastrophic failure under extreme conditions.

3.3. Solution Strategy for Minimax Regret Optimization Problem via Benders Decomposition

The problem involves coupled investment-operation timescales and a nested minimax structure, where the operational cost $Q_{s,p}(X)$ is an implicit function of the investment decision X, making direct solution computationally prohibitive. To maintain solvability and computational efficiency in large-scale power grid contexts, an improved Benders decomposition is thus employed, decoupling the problem into an investment master problem (MP) and an operation subproblem (SP). Specifically, The MP determines a system-wide capacity plan to minimize the maximum regret, while the SP, solved by the SWITCH model, assesses this portfolio across diverse extreme climate scenarios and feeds operational constraints back as Benders cuts. By iteratively incorporating these dynamically generated cuts into the MP, the algorithm progressively refines the approximation of the true regret cost curve. The detailed mathematical formulations, derivations of the optimality cuts, convergence proofs, and pseudocode are detailed in Appendix D.

4. Case Study

4.1. Lvliang Data Description

We validate the proposed framework through a case study of Lvliang City, Shanxi Province. Initial hourly demand profiles for 2025 are derived by downscaling provincial macroeconomic projections from the National Development and Reform Commission (NDRC) (National Development and Reform Commission, 2019). For subsequent periods, hourly load profiles under different climate states are dynamically predicted by Bi-LSTM model. This ensures strict synchronization with the meteorological scenarios generated by the GNN-cGAN, effectively capturing the non-linear climate-demand coupling.

To generate the synthetic wind, temperature, and solar profiles required for capacity expansion simulations, we train the GNN-cGAN model utilizing 25 years (2000–2024) of meteorological reanalysis records from the ERA5 dataset (Muñoz Sabater, 2019) and the National Climate Center (National Climate Center, 2024). Furthermore, to accurately capture nonlinear load surges during extreme weather events, we incorporate a physical correction mechanism based on temperature sensitivity. This mechanism calibrates demand responses to heatwaves and cold spells in accordance with local heating and cooling policies.

On the supply side, technical parameters for thermal units are sourced from the Global Coal Plant Tracker dataset (Global Energy Monitor, 2024), while renewable potentials are constrained by regional land-use data. Additionally, we explicitly model industrial Demand Response (DR), scaling its available capacity based on the economic footprint of Lvliang's energy-intensive sectors (e.g., electrolytic aluminum processing) as reported in the Lvliang Statistical Yearbook (Lvliang Municipal Bureau of Statistics, 2020). Detailed parameter settings are provided in Appendix E.

4.2. Validation of Extreme Scenario Generation

To verify the fidelity of GNN-cGAN generated scenarios, we conduct multi-dimensional comparisons between the generated scenarios and ERA5 reanalysis data (2000–2024) (Muñoz Sabater, 2019). We use Wasserstein Distance (WD) to quantify distributional discrepancies, with the normalized relative error (RE) defined as $\mathrm{RE} = \frac{\mathrm{WD}_{Score}}{D_{max} - D_{min}}$, where D_{max} and D_{min} are the physical boundaries of each variable.

As shown in Fig. 4, the model accurately preserves key physical couplings, such as temperature-irradiance (Real: 0.41 vs. Gen: 0.44) and wind-irradiance correlations (Real: 0.39 vs. Gen: 0.46), while maintaining near-zero coefficients for weakly correlated features. Furthermore, Fig. 5 and Table 1 demonstrate that the generated distributions closely align with historical ground truth. All RE values remain below 4%, confirming that the GNN-cGAN can generate physically consistent and statistically high-fidelity extreme states that exceed routine operational ranges.

Table 1: WD Score and Error Metrics for Key Variables.

Variable	WD Score	Data Range	Relative Error
rsds	18.48	$0 \sim 1012$	1.83%
temp_c	2.00	-23 $\sim$ 38	3.28%
v80m	0.59	$0 \sim 24$	2.46%
pr	0.40	$0 \sim 10$	4.00%

4.3. Robustness Assessment and Cost-Reliability Trade-off Analysis

To rigorously evaluate planning scenario performance and vulnerability, this section conducts a multi-dimensional operational stress test.Here, we define Deterministic (DET) models as benchmark solutions optimized for a single climate trajectory with perfect foresight. The 27 generated pathways are categorized into two groups: 9 "Grim

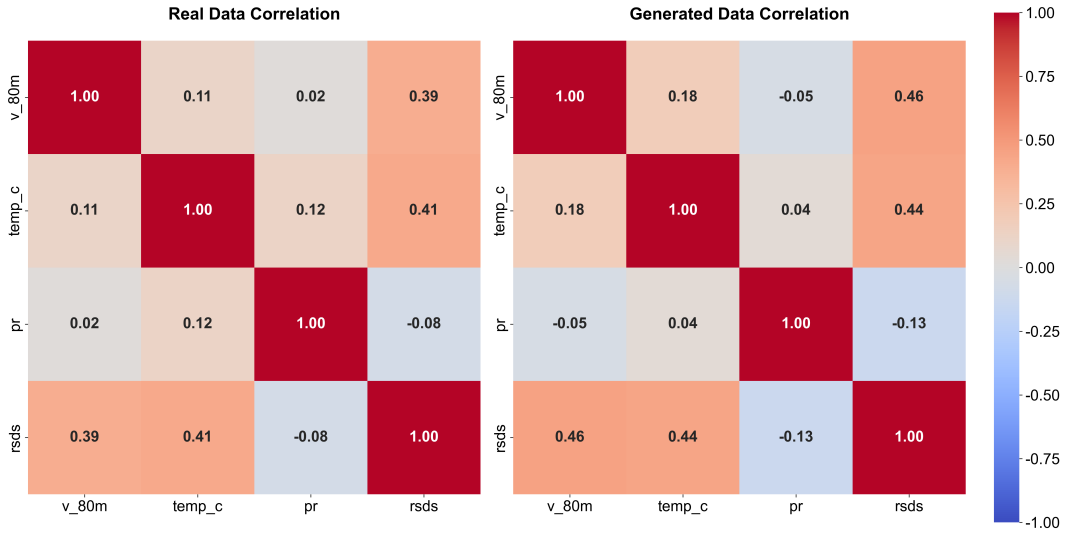

Figure 4: Verification of physical coupling characteristics.

Scenarios" that begin with Extremely Cold Year (ECY) in 2030, representing periods of high demand and low VRE availability, while 18 "Gentle Scenarios" begin with Typical or Extremely Warm Years (TDY/EWY). This division enables targeted assessment of the MMR scenario's resilience against high-risk, coupled supply-demand imbalances, comparing it against DET benchmarks specifically for grim or gentle conditions. Fig. 6 illustrates the regret distribution for the MMR model and all 27 DET configurations. Serving as a direct metric for robustness, the regret values clearly validate the superiority of the MMR framework in mitigating risk. The MMR regret distribution exhibits a highly concentrated spread, with a maximum regret substantially lower than that of any DET counterpart. This confirms that strategic hedging during the initial investment stage successfully constrains risk exposure across most potential climate evolution paths, ensuring robust decisions under deep uncertainty.

To evaluate the performance of the MMR scenario under different macro-climate scenarios, we benchmark it against three representative DET solutions at the initial 2030 decision node: DET^{CTT}, DET^{TTT}, and DET^{WTT}. These benchmarks assume typical data years for subsequent periods, which isolates the impact of the initial 2030 climate shock on long-term investment robustness (full results for all 27 pathways are provided in Appendix G). Fig. 7 illustrates the cumulative installed capacity configuration of the four planning scenarios at different decision nodes, the capacity configuration of the DET scenarios exhibits significant path lock-in risks, as their capacity expansion strategies are highly dependent on the initial climate state assumed in 2030. The investment in grim scenarios prioritizes winter supply reliability, which results in a massive wind power capacity surge in 2030. However, this scenario suffers from severe investment stagnation, with no additional capacity expansion from 2030 to 2040. In contrast, decisions guided by optimistic scenarios reflect a conservative investment logic focused on minimizing upfront costs, resulting in persistently low capacity expansion and delayed resource deployment (e.g. the DET^{TTT} scenario). By maintaining a balanced wind-solar-storage mix from the outset and leveraging resource complementarity, the MMR scenario strengthens resilience and sustains continuous growth rather than reactive, "one-off" adjustments, which

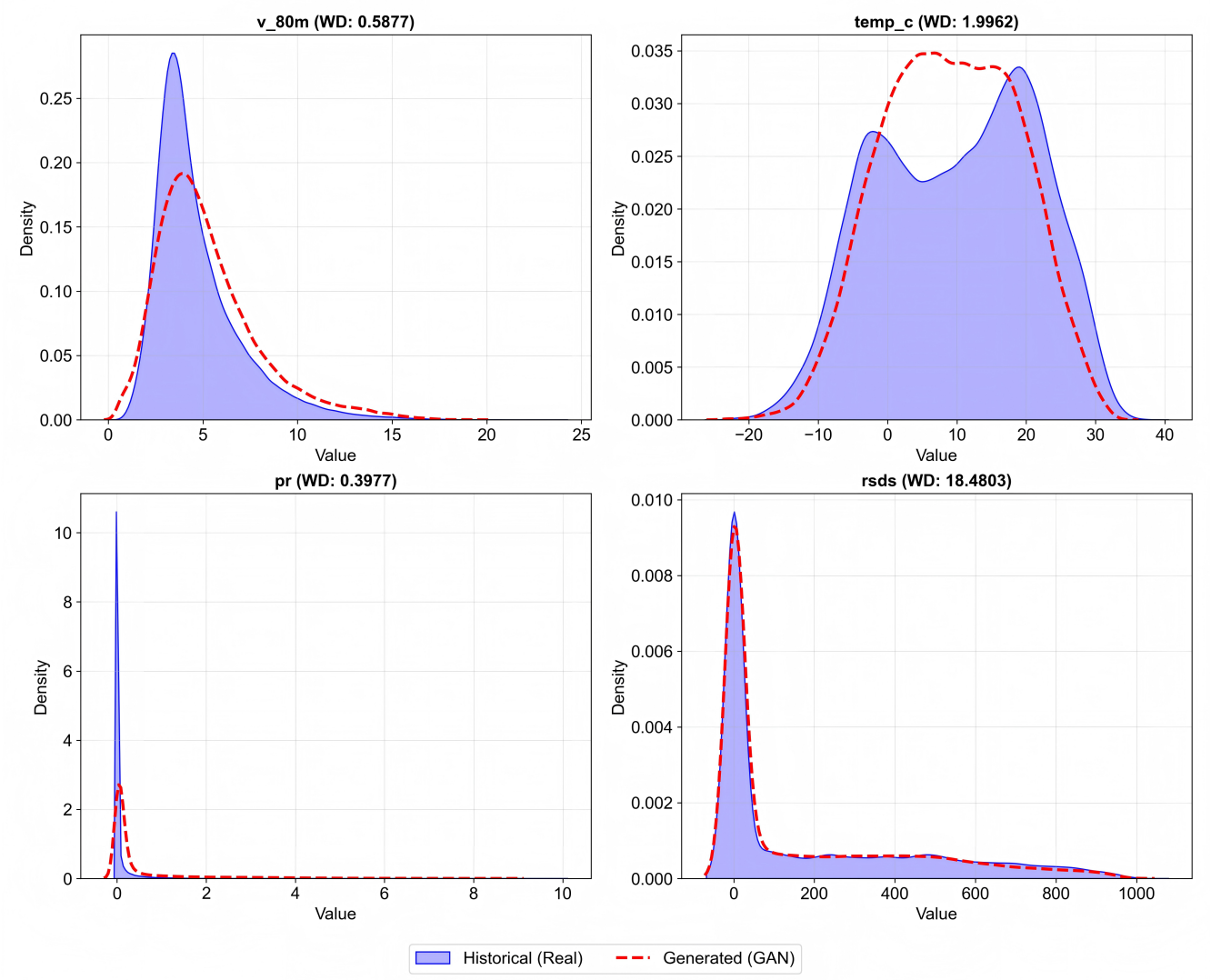

Figure 5: Comparison of probability density curves between real data and generated data.

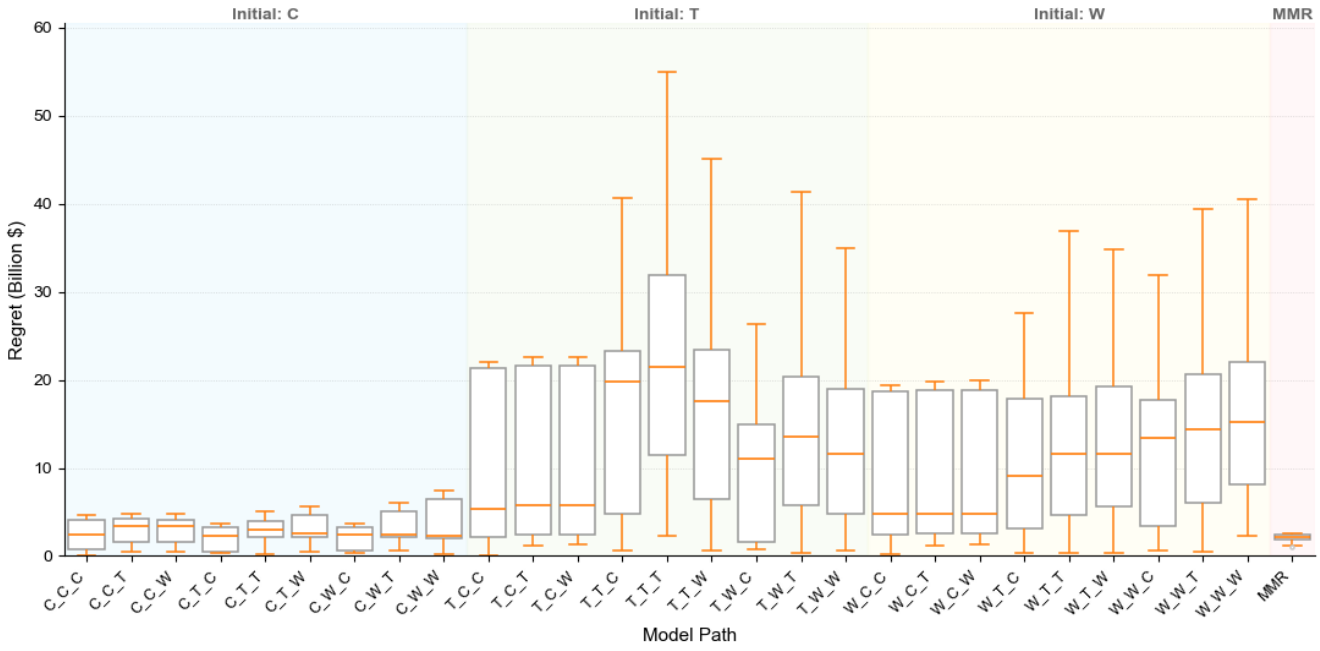

Figure 6: Regret value comparison diagram between MMR and DET models across climate pathways.

can avoid path lock-in within deterministic planning.

To quantitatively assess the reliability level of planning scenarios over the entire lifecycle, we define the Unserved Electricity Rate (UER) as the ratio of the system's cumulative energy not served (ENS) to the total electricity demand (Load_Demand) during the evaluation period. Through a normalization process, this metric eliminates the influence of differences in load scale, thereby intuitively reflecting the relative severity of the system's supply-demand imbalance:

$$\mathrm{UER} = \frac{\sum \mathrm{ENS}}{\sum \mathrm{Load\_Demand}} \times 100\% \tag{8}$$

A comprehensive comparison of the physical reliability metrics, specifically the maximum and mean UER across all 27 DET benchmark solutions, is further elaborated in Appendix H. This detailed evaluation provides evidence of the resilience collapse inherent in deterministic models under non-designed climate pathways.

Figure 8 illustrates the performance shifts, comparing the total cost change (calculated as $\mathrm{Cost}_{\mathrm{MMR}} - \mathrm{Cost}_{\mathrm{DET}}$ on the x-axis) and the UER reduction (calculated as $\mathrm{UER}_{\mathrm{MMR}} - \mathrm{UER}_{\mathrm{DET}}$ on the y-axis) of the MMR scenario relative to three specific DET baselines across all 27 climate pathways: $\mathrm{Path}^{\mathrm{TTT}}$ (green), $\mathrm{Path}^{\mathrm{WTT}}$ (red), and $\mathrm{Path}^{\mathrm{CTT}}$ (blue). All scatter plots exhibit a strong positive correlation trend in terms of reductions, meaning a greater cost saving by the MMR scenario (negative x-axis) corresponds to a more significant reliability improvement (negative y-axis), which visually demonstrates the MMR solution's capability in mitigating high-risk events across different strategic trajectories. This counter-intuitive correlation highlights the core economic value of robust planning in defending against extreme events. Notably, in the comparison with $\mathrm{DET}^{\mathrm{TTT}}$, the MMR scenario achieves extreme net savings of over \$50 billion and a 10% reduction in UER on the most critical paths. The overwhelming concentration of data

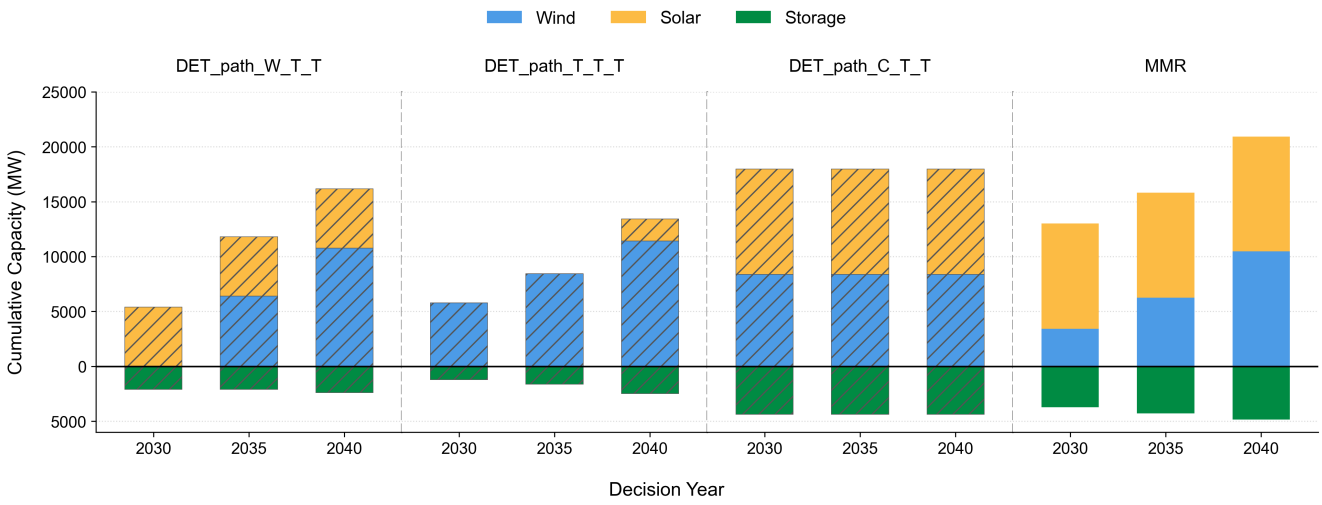

Figure 7: Comparison of cumulative installed capacity expansion between MMR and representative deterministic baselines.

points in the third quadrant (lower-left) for typical and warm baselines demonstrates that MMR is not merely a trade-off, but a Pareto-dominant solution that is simultaneously more economical and more resilient under climate stress.

4.4. Out-of-sample Stability and Cross-Validation Analysis

To ensure that the superior performance of the MMR scenario is not biased by the specific stochastic realizations of the initial 27 scenarios (Set 1), we conduct a 5-fold out-of-sample stability test. The optimal investment decision X^* derived from Set 1 is stress-tested against four additional, independently generated climate scenario sets (Set 2-5). Fig. 9a reveals that the MMR scenario (red) consistently constrains both the maximum UER (bars) and mean UER (dots) within a remarkably low range ($< 3.2\%$) across all validation sets. Fig. 9b demonstrates the economic robustness of the MMR decision. The regret distributions for MMR are notably compact and positioned near the zero-baseline, indicating that the robust hedging strategy maintains high economic efficiency regardless of stochastic fluctuations in climate variables. In contrast, deterministic scenarios exhibit high variance and significant tail risks.

To further quantify the optimality gap of the out-of-sample decision, Fig. 10 compares the performance of the Set 1 solution (orange) against the self-optimal performance (grey) specifically optimized for each validation set. The high degree of overlap between the orange and grey boxplots across Sets 2-5 provides definitive evidence of the generalization capability of the MMR scenario. The regret increment remains minimal (mean gap $<$ \$0.5 billion), suggesting that the decision boundaries captured from the generative-adversarial training effectively reflect the universal risk structure of the local climate-energy nexus, without overfitting to specific scenario sequences. These consistent results statistically eliminate the accidental effects of scenario sampling. The proposed methodology can ensure city level energy systems remain both economically efficient and physically reliable regardless of the specific stochastic implementation of future climate extremes.

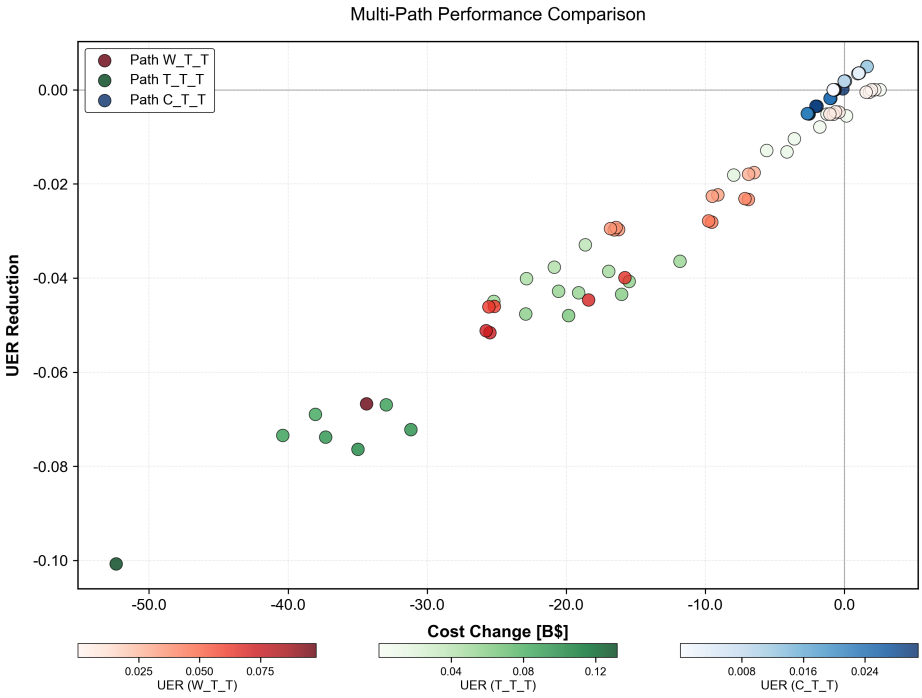

Figure 8: Comparison of MMR solution robustness and cost-reliability trade-offs relative to representative deterministic baselines.

Figure 9: Cross-validation analysis of reliability and economic performance across independent validation sets. (a) Consistency of unserved energy rates showcasing maximum (bars) and mean (dots) values; (b) Distribution of economic regrets among deterministic and robust modeling approaches.

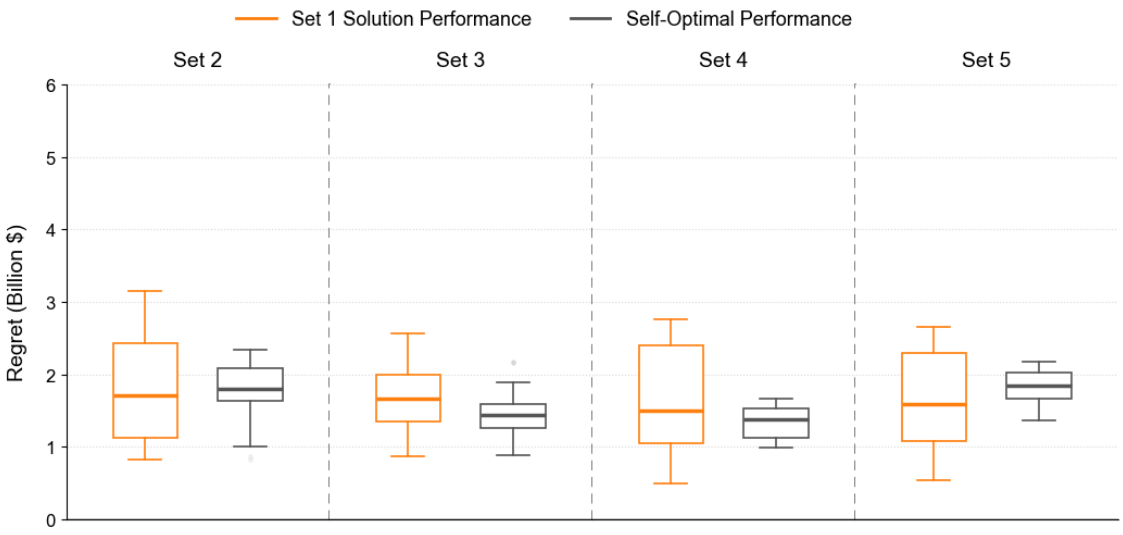

Figure 10: Generalization capability of the fixed training-set decision against set-specific optimal benchmarks.

5. Conclusion

We present an integrated framework that leverages GNN-cGAN scenario generation and MMR optimization to mitigate non-stationary climate risks in city's power system planning. The modular architecture structurally decouples uncertainty generation from the operational solver, enabling the upgrade of all existing deterministic power system planning frameworks for climate resilience without fundamental reformulations. The integration of GNN-cGAN into a 27-path scenario tree allows for the systematic endogenization of long-tail climate risks and compound extremes. This framework ensures that resulting planning decisions possess both physical feasibility and economic robustness.

The case study in Lvliang demonstrates that deterministic models face significant resilience vulnerabilities, with the UER exceeding 13% under extreme climate trajectories that deviate from their simplified assumptions. Conversely, the MMR scenario effectively avoids investment lock-in and constrains maximum risk exposure by strategically deploying energy storage and demand-side flexibility. Quantitative analysis confirms that MMR acts as a Pareto-dominant solution, achieving an average net cost saving of 14.04% (up to 55.95%) and demonstrating superior economic performance in 74.62% of the 729 (27×27) evaluated climate trajectories by avoiding exorbitant penalty costs during extreme events.

Several caveats regarding the scope and data dependencies of this study should be addressed. The current framework relies on historical reanalysis data, which may not capture unprecedented local micro-climate shifts. Additionally, the scenario generation primarily focuses on temperature-driven compound extremes, while these are critical for urban peak-load management, future enhancements should incorporate other climate-driven risks such as prolonged droughts or extreme precipitation. This research shifts the planning paradigm from capacity-driven expansion to resource complementarity, proving that a moderate robustness premium is economically superior for long-term stability. The proposed methodology is particularly applicable to resource-dependent regions undergoing

high-VRE transitions. Future work will extend this framework to incorporate urbanization impacts and multi-regional collaborative flexibility mechanisms under cross-regional interconnection.

References

Alqurashi, A., Etemadi, A.H., Khodaei, A., 2016. Treatment of uncertainty for next generation power systems: State-of-the-art in stochastic optimization. Electr. Power Syst. Res. 141, 233–45. https://doi.org/10.1016/j.epsr.2016.08.007.

Asadoorian, M.O., Eckaus, R.S., Schlosser, C.A., 2008. Modeling climate feedbacks to electricity demand: The case of china. Energy Econ. 30, 1577–602. https://doi.org/10.1016/j.eneco.2008.01.002.

Bennett, J.A., Trevisan, C.N., DeCarolis, J.F., et al., 2021. Extending energy system modelling to include extreme weather risks and application to hurricane events in puerto rico. Nat. Energy 6, 240–9. https://doi.org/10.1038/s41560-020-00758-5.

Cao, X., Wang, J., Zeng, B., 2018. A chance constrained information-gap decision model for multi-period microgrid planning. IEEE Trans. Power Syst. 33, 2684–95. https://doi.org/10.1109/TPWRS.2017.2754642.

Chen, B., Liu, T., Liu, X., et al., 2022. Distributionally robust coordinated expansion planning for generation, transmission, and demand side resources considering the benefits of concentrating solar power plants. IEEE Trans. Power Syst. 38, 1205–18. https://doi.org/10.1109/TPWRS.2022.3168249.

Chen, H., Yan, H., Gong, K., et al., 2021. How will climate change affect the peak electricity load? evidence from china. J. Clean. Prod. 322, 129080. https://doi.org/10.1016/j.jclepro.2021.129080.

Chen, Y., Wang, Y., Kirschen, D., et al., 2019. Model-free renewable scenario generation using generative adversarial networks, in: Proc. 2019 IEEE Power Energy Soc. Gen. Meet. (PESGM), p. 1. https://doi.org/10.1109/PESGM40551.2019.8974096.

Conejo, A.J., Wu, X., 2022. Robust optimization in power systems: A tutorial overview. Optim. Eng. 23, 2051–73. https://doi.org/10.1007/s11081-021-09658-y.

Deng, A., Hooi, B., 2021. Graph neural network-based anomaly detection in multivariate time series, in: Proc. AAAI Conf. Artif. Intell., pp. 4027–35. https://doi.org/10.1609/aaai.v35i5.16523.

Denholm, P., Hand, M., 2011. Grid flexibility and storage required to achieve very high penetration of variable renewable electricity. Energy Policy 39, 1817–30. https://doi.org/10.1016/j.enpol.2011.01.033.

Diaz, G., Gomez-Aleixandre, J., Coto, J., 2016. Wind power scenario generation through state-space specifications for uncertainty analysis of wind power plants. Appl. Energy 162, 21–30. https://doi.org/10.1016/j.apenergy.2015.10.046.

Dong, C., Huang, G.H., Cai, Y.P., et al., 2011. An interval-parameter minimax regret programming approach for power management systems planning under uncertainty. Appl. Energy 88, 2835–45. https://doi.org/10.1016/j.apenergy.2011.01.029.

Dupačová, J., 2002. Applications of stochastic programming: Achievements and questions. Eur. J. Oper. Res. 140, 281–90. https://doi.org/10.1016/S0377-2217(02)00063-2.

Fan, J.L., Hu, J.W., Zhang, X., 2019. Impacts of climate change on electricity demand in china: An empirical estimation based on panel data. Energy 170, 880–8. https://doi.org/10.1016/j.energy.2018.12.146.

Fang, P., Wang, T., Yang, D., et al., 2025. Substantial increases in compound climate extremes and associated socio-economic exposure across china under future climate change. npj Clim. Atmos. Sci. 8, 17. https://doi.org/10.1038/s41612-025-00910-7.

Gao, H., Liu, J., Wang, L., 2018. Robust coordinated optimization of active and reactive power in active distribution systems. IEEE Trans. Smart Grid 9, 4436–47. https://doi.org/10.1109/TSG.2017.2657778.

Ghodeswar, A., Bhandari, M., Hedman, B., 2025. Quantifying the economic costs of power outages owing to extreme events: A systematic review. Renew. Sustain. Energy Rev. 207, 114984. https://doi.org/10.1016/j.rser.2024.114984.

Giannelos, S., Konstantelos, I., Strbac, G., 2018. Option value of demand-side response schemes under decision-dependent uncertainty. IEEE Trans. Power Syst. 33, 5103–13. https://doi.org/10.1109/TPWRS.2018.2816748.

Global Energy Monitor, 2024. [dataset] global coal plant tracker. URL: https://globalenergymonitor.org/projects/global-coal-plant-tracker/. accessed 20 May 2024.

Gu, C., Ruan, J., Qiu, Y., et al., 2026. Toward climate-adaptive low-carbon power system planning: A multistage stochastic framework considering climate uncertainties. IEEE Trans. Ind. Informatics , 1–12https://doi.org/10.1109/TII.2026.3653787.

He, G., Avrin, A.P., Nelson, J.H., et al., 2016. SWITCH-china: A systems approach to decarbonizing china's power system. Environ. Sci. Technol. 50, 5467–73. https://doi.org/10.1021/acs.est.6b01046.

Hirth, L., Ziegenhagen, I., 2015. Balancing power and variable renewables: Three links. Renew. Sustain. Energy Rev. 50, 1035–51. https://doi.org/10.1016/j.rser.2015.04.180.

Impram, S., Varbak Nese, S., Oral, B., 2020. Challenges of renewable energy penetration on power system flexibility: A survey. Energy Strategy Rev. 31, 100539. https://doi.org/10.1016/j.esr.2020.100539.

Jasiūnas, J., Lund, P.D., Mikkola, J., et al., 2021. Linking socio-economic aspects to power system disruption models. Energy 222, 119928. https://doi.org/10.1016/j.energy.2020.119928.

Jiang, R., Wang, J., Zhang, M., et al., 2013. Two-stage minimax regret robust unit commitment. IEEE Trans. Power Syst. 28, 2271–82. https://doi.org/10.1109/TPWRS.2012.2230275.

Johnston, J., Henriquez-Auba, R., Maluenda, B., et al., 2019. Switch 2.0: A modern platform for planning high-renewable power systems. SoftwareX 10, 100251. https://doi.org/10.1016/j.softx.2019.100251.

Khodaei, A., Bahramirad, S., Shahidehpour, M., 2015. Microgrid planning under uncertainty. IEEE Trans. Power Syst. 30, 2417–25. https://doi.org/10.1109/TPWRS.2014.2361034.

Kipf, T.N., Welling, M., 2017. Semi-supervised classification with graph convolutional networks, in: Proc. Int. Conf. Learn. Represent. (ICLR). https://openreview.net/forum?id=SJU4ayYgl.

Kjølle, G.H., Utne, I.B., Gjerde, O., 2012. Risk analysis of critical infrastructures emphasizing electricity supply and interdependencies. Reliab. Eng. Syst. Saf. 105, 80–9. https://doi.org/10.1016/j.ress.2012.03.015.

Konstantelos, I., Strbac, G., 2015. Valuation of flexible transmission investment options under uncertainty. IEEE Trans. Power Syst. 30, 1047–55. https://doi.org/10.1109/TPWRS.2014.2335418.

Lai, G., Chang, W.C., Yang, Y., et al., 2018. Modeling long- and short-term temporal patterns with deep neural networks, in: Proc. 41st Int. ACM SIGIR Conf. Res. Dev. Inf. Retr., pp. 95–104. https://doi.org/10.1145/3209978.3210006.

Li, Y., Yu, R., Shahabi, C., et al., 2018. Diffusion convolutional recurrent neural network: Data-driven traffic forecasting, in: Proc. Int. Conf. Learn. Represent. (ICLR). https://openreview.net/forum?id=SJiZ619Sg.

Liu, Y., Guo, L., Hou, R., et al., 2021. A hybrid stochastic/robust-based multi-period investment planning model for island microgrid. Int. J. Electr. Power Energy Syst. 130, 106998. https://doi.org/10.1016/j.ijepes.2021.106998.

Lund, P.D., Lindgren, J., Mikkola, J., et al., 2015. Review of energy system flexibility measures to enable high levels of variable renewable electricity. Renew. Sustain. Energy Rev. 45, 785–807. https://doi.org/10.1016/j.rser.2015.01.057.

Lvliang Municipal Bureau of Statistics, 2020. Lvliang Statistical Yearbook 2020. China Statistics Press, Beijing. In Chinese.

Morales, J.M., Minguez, R., Conejo, A.J., 2010. A methodology to generate statistically dependent wind speed scenarios. Appl. Energy 87, 843–55. https://doi.org/10.1016/j.apenergy.2009.08.021.

Muñoz Sabater, J., 2019. [dataset] ERA5-Land hourly data from 1950 to present. doi:10.24381/cds.e2161bac. accessed 20 May 2024.

National Climate Center, 2024. [dataset] historical meteorological records of china. Internal database.

National Development and Reform Commission, 2019. [dataset] provincial macroeconomic projections. URL: http://www.ndrc.gov.cn/xxgk/zcfb/tz/201912/t20191230_1216857.html. accessed 20 May 2024.

Nik, V.M., Perera, A.T.D., Chen, D., 2021. Towards climate resilient urban energy systems: a review. Natl. Sci. Rev. 8, nwaa134. https://doi.org/10.1093/nsr/nwaa134.

Panteli, M., Pickering, C., Wilkinson, S., et al., 2017. Power system resilience to extreme weather: Fragility modeling, probabilistic impact assessment, and adaptation measures. IEEE Trans. Power Syst. 32, 3747–57. https://doi.org/10.1109/TPWRS.2016.2630309.

Paredes-Vergara, M., Cerda-Arias, J.L., Palma-Behnke, R., Haas, J., 2025. A framework for integrating deep uncertainty in power systems planning: an application to the chilean case. Appl. Energy 398, 126437. https://doi.org/10.1016/j.apenergy.2025.126437.

Perera, A.T.D., Nik, V.M., Chen, D., et al., 2020. Quantifying the impacts of climate change and extreme climate events on energy systems. Nat. Energy 5, 150–9. https://doi.org/10.1038/s41560-020-0548-8.

Qiu, H., Wang, Z., He, S., 2023. Separation in distributionally robust monopolist problem, in: Proc. Web and Internet Economics (WINE 2023), Springer, Cham. pp. 545–62. https://doi.org/10.1007/978-3-031-48974-7_34.

Shair, J., Li, H., Hu, J., et al., 2021. Power system stability issues, classifications and research prospects in the context of high-penetration of renewables and power electronics. Renew. Sustain. Energy Rev. 145, 111111. https://doi.org/10.1016/j.rser.2021.111111.

Sinsel, S.R., Riemke, R.L., Hoffmann, V.H., 2020. Challenges and solution technologies for the integration of variable renewable energy sources—a review. Renew. Energy 145, 2271–85. https://doi.org/10.1016/j.renene.2019.06.147.

Stürmer, J., Plietzsch, A., Vogt, T., et al., 2024. Increasing the resilience of the texas power grid against extreme storms by hardening critical lines. Nat. Energy 9, 526–35. https://doi.org/10.1038/s41560-024-01503-x.

Wang, H., Qin, B., Hong, S., et al., 2025. Enhanced gan-based joint wind-solar-load scenario generation with extreme weather labelling. IEEE Trans. Smart Grid 16, 4213–24. https://doi.org/10.1109/TSG.2024.3401234.

Wang, Y., Liu, Y., Yang, Q., 2023. Operational scenario generation and forecasting for integrated energy systems. IEEE Trans. Ind. Informatics 20, 2920–31. https://doi.org/10.1109/TII.2023.3305678.

Wu, Z., Pan, S., Long, G., et al., 2020. Connecting the dots: Multivariate time series forecasting with graph neural networks, in: Proc. 26th ACM SIGKDD Int. Conf. Knowl. Discov. Data Min., pp. 753–63. https://doi.org/10.1145/3394486.3403118.

Xie, S., Hu, Z., Wang, J., 2020. Two-stage robust optimization for expansion planning of active distribution systems coupled with urban transportation networks. Appl. Energy 261, 114412. https://doi.org/10.1016/j.apenergy.2019.114412.

Xu, L., Lin, N., Poor, H.V., et al., 2025. Quantifying cascading power outages during climate extremes considering renewable energy integration. Nat. Commun. 16, 2582. https://doi.org/10.1038/s41467-025-57565-4.

Yang, N., Wen, F., 2005. A chance constrained programming approach to transmission system expansion planning. Electr. Power Syst. Res. 75, 171–7. https://doi.org/10.1016/j.epsr.2005.02.005.

Yang, S., Jahanger, A., Awan, A., 2024. Temperature variation and urban electricity consumption in china: Implications for demand management and planning. Util. Policy 90, 101782. https://doi.org/10.1016/j.jup.2024.101782.

Yazdani, D., Omidvar, M.N., Yazdani, D., et al., 2023. Robust optimization over time: A critical review. IEEE Trans. Evol. Comput. 28, 1265–85. https://doi.org/10.1109/TEVC.2023.3283344.

Yu, B., Yin, H., Zhu, Z., 2018. Spatio-temporal graph convolutional networks: A deep learning framework for traffic forecasting, in: Proc. 27th Int. Joint Conf. Artif. Intell. (IJCAI), pp. 3634–40. https://doi.org/10.24963/ijcai.2018/505.

Zhao, N., You, F., 2021. New york state's 100% renewable electricity transition planning under uncertainty using a data-driven multistage adaptive robust optimization approach with machine-learning. Adv. Appl. Energy 2, 100019. https://doi.org/10.1016/j.adapen.2021.100019.

Zheng, D., Yan, X., Tong, D., et al., 2025. Strategies for climate-resilient global wind and solar power systems. Nature 643, 1263–70. https://doi.org/10.1038/s41586-025-09266-7.

Zheng, S., Huang, G., Zhou, X., et al., 2020. Climate-change impacts on electricity demands at a metropolitan scale: A case study of guangzhou, china. Appl. Energy 261, 114295. https://doi.org/10.1016/j.apenergy.2019.114295.

Zhuang, L., Wang, M., Liu, K., et al., 2026. Assessing and optimizing urban dynamic resilience to extreme rainfall from shock to recovery. Int. J. Disaster Risk Sci. 17, 128–47. https://doi.org/10.1007/s13753-025-00683-w.

Appendix A. The SWITCH Power System Planning Model

The SWITCH model is an open-source mixed-integer linear programming platform dedicated to the capacity expansion and operational planning of low-emission power systems. It provides a high degree of flexibility, allowing users to construct customized power system models by selecting built-in modules or developing new ones to suit specific research requirements (Johnston et al., 2019).

To maintain conciseness, this section outlines the core mathematical formulation and the customized modules developed specifically for this study. Comprehensive algebraic formulations, including granular capacity accumulation, local transmission and distribution (T&D) accounting, and detailed financial discounting mechanisms—are available in the official SWITCH GitHub repository (`https://github.com/switch-model/switch`).

Appendix A.1. Core Objective and Basic Constraints

The fundamental objective of the SWITCH model is to minimize the net present value (NPV) of the total system costs, which comprise annualized fixed capital/O&M costs (C^{fixed}) and variable operational/fuel costs (C^{var}):

$$\min \sum_{p \in \mathcal{P}} d_p \left\{ \sum_{c \in \mathcal{C}^{\text{fixed}}} c_{c,p}^{\text{fixed}} + \sum_{t \in \mathcal{T}, c \in \mathcal{C}^{\text{var}}} w_t^{\text{year}} c_{c,t}^{\text{var}} \right\} \tag{A.1}$$

where d_p and w_t^{year} are the corresponding discount and temporal weighting factors, respectively.

This cost minimization is subject to a suite of rigorous physical and policy constraints. The most critical constraint is the nodal power balance, which ensures that total power injections equal total power withdrawals at each load zone z and timepoint t:

$$\sum P_{z,t}^{\text{inject}} = \sum P_{z,t}^{\text{withdraw}}, \quad \forall z \in \mathcal{Z}, \forall t \in \mathcal{T} \tag{A.2}$$

Additionally, generation and transmission power flows are constrained by their respective cumulative installed capacities and temporal availability factors (e.g., dynamic capacity factors for variable renewable energy). To align with climate targets, the system-wide carbon emissions are strictly constrained by a predefined annual emissions cap:

$$\text{AnnualEmissions}_p \leq \text{cap}_p^{\text{c}}, \quad \forall p \in \mathcal{P} \tag{A.3}$$

Appendix A.2. Customized Combined Heat and Power (CHP) Module

While SWITCH provides comprehensive standard modules, it lacks endogenous representations of waste heat utilization. To incorporate the utilization of waste heat from combined heat and power (CHP) systems, this study introduces a newly developed `cogen` module. This module defines additional dispatch constraints to optimize the investment and operation of CHP units.

In each period, the total available capacity of a CHP unit is tracked dynamically. The electricity generation from CHP units is strictly bounded by the available waste heat. Consequently, the thermal energy consumed for power generation must not exceed the total waste heat available at any given time:

$$\text{DispatchCogen}_{g,t} \leq \text{CogenCapacity}_{g,p} \tag{A.4}$$

$$\text{DispatchCogen}_{g,t} \times \text{cogen\_heat\_rate} \leq \text{heat\_input}_{g,t} - \text{work\_done}_{g,t} \tag{A.5}$$

$$\text{heat\_input}_{g,t} = P^{\text{G}}_{g,t} \times h_g \tag{A.6}$$

$$\text{work\_done}_{g,t} = P^{\text{G}}_{g,t} \times 3.412 \tag{A.7}$$

Here, `cogen_heat_rate` represents the heat rate of the CHP unit, defined as the thermal energy input (in MMBtu) required to generate one megawatt-hour (MWh) of electricity. $\text{heat\_input}_{g,t}$ is the total available waste heat for CHP plant g at timepoint t. $\text{work\_done}_{g,t}$ represents the thermal energy converted to electricity, where 3.412 is the physical conversion factor from MMBtu to MWh. The annualized fixed costs associated with the built `cogen` capacity are subsequently integrated into the C^{fixed} term of the primary objective function.

Appendix B. Mathematical Formulation of the GNN-cGAN Model

The multivariate time series is abstracted as a dynamic correlation graph $\mathcal{G}(t) = (\mathcal{V}, \mathcal{E}, W)$, where nodes $v \in \mathcal{V}$ represent meteorological variables (wind, temperature, etc.) and edges $e \in \mathcal{E}$ capture their physical couplings.

Generator Architecture: For each time step t, the scalar observation $s_{i,t}$ is first mapped to a high-dimensional latent space $h^0_{i,t} \in \mathbb{R}^{d_k}$. To capture non-linear inter-variable dependencies, a Graph Attention Network (GAT) computes the dynamic spatial features $h^{\text{spat}}_{i,t}$:

$$h^{\text{spat}}_{i,t} = \sigma\left(\sum_{j \in \mathcal{N}_i} \alpha_{ij,t} W_v h^0_{j,t}\right) \tag{B.1}$$

where the attention coefficients $\alpha_{ij,t}$ are derived via the LeakyReLU-Softmax mechanism based on the hidden states of node pairs (i, j). These spatially-fused features are then fed into a Gated Recurrent Unit (GRU) to decode temporal dependencies:

$$H_{i,t} = \text{GRU}(h^{\text{spat}}_{i,t}, H_{i,t-1}) \tag{B.2}$$

The final generated value $\tilde{s}_{i,t}$ is obtained by mapping $H_{i,t}$ back to the physical space.

Discriminator and Loss Functions: The discriminator D utilizes a symmetric GAT-BiGRU architecture to extract spatio-temporal features $F_{\text{spat}-\text{temp}}$ from either real or synthetic sequences. To stabilize training and enhance physical fidelity, we employ the WGAN-GP objective supplemented by a Feature Matching (FM) loss:

$$\mathcal{L} = \mathbb{E}_{\tilde{x} \sim P_g}[D(\tilde{x})] - \mathbb{E}_{x \sim P_r}[D(x)] + \lambda_{\text{gp}} \mathcal{L}_{\text{GP}} + \lambda_{\text{FM}} \left\| \mathbb{E}_{x \sim P_r}[\psi(x)] - \mathbb{E}_{\tilde{x} \sim P_g}[\psi(\tilde{x})] \right\|_2^2 \tag{B.3}$$

where $\mathcal{L}_{\text{GP}}$ is the gradient penalty and $\psi(\cdot)$ represents the intermediate feature mapping of D. This dual-loss structure encourages the generator to replicate both the probability density and the statistical moments of real-world meteorological processes.

Appendix C. Technical Details of Load Forecasting and Renewable Capacity Factor Calculation

To predict hourly electric load curves corresponding to these scenarios with physical consistency, we constructed a dedicated pure weather-driven deep learning model based on Bidirectional Long Short-Term Memory (Bi-LSTM) networks, thereby replacing traditional autoregressive frameworks. Crucially, the model strictly excludes historical load lag features, relying only on key meteorological variables and their non-linear derivatives as inputs. Furthermore, it incorporates sine-cosine positional encoding and a virtual social clock encoding to effectively capture the temporal regularities of load variations. This approach enables the prediction of hourly electric load curves corresponding to specific scenarios.

We define the pure weather-driven forecasting function F_θ as follows:

$$L_t = F_\theta(M_t, T_t) \tag{C.1}$$

$$M_t = [S_t, S_{t-w:t}, \Delta S_t] \tag{C.2}$$

where L_t denotes the predicted electric load at time step t. M_t represents the augmented meteorological feature vector, and T_t is the temporal encoding vector. $S_{t-w:t}$ represents the rolling mean over a window w (set to 6 hours in this study) to capture thermal accumulation effects; and ΔS_t denotes the first-order difference representing rapid weather changes. The temporal encoding vector T_t embeds the cyclic nature of human activities using sine-cosine transformations and social clock indicators:

$$T_t = \left[\sin\left(\frac{2\pi h_t}{24}\right), \cos\left(\frac{2\pi h_t}{24}\right), I_{weekday}, I_{holiday}\right] \tag{C.3}$$

where h_t is the hour of the day, and I represents the indicator function for workdays and holidays. In the model training phase, Mean Squared Error (MSE) is selected as the loss function:

$$\mathcal{L}_{MSE} = \frac{1}{N}\sum_{i=1}^{N}(L_i - \hat{L}_i)^2 \tag{C.4}$$

Simultaneously, the model integrates scenario data to calculate the time-series capacity factors for wind turbines and PV power stations. The final model architecture underwent systematic hyperparameter optimization; the parameters of the optimized model structure are detailed in Table C.2.

To calculate the hourly capacity factors for wind and solar power generation, the following mathematical formulations are employed:

$$REcf_{n,wind,c} = \begin{cases} 0 & v_{n,c} \le v_{in} \text{ or } v_{n,c} \ge v_{out} \\ (\eta T_{n,c} + k)\frac{v_{n,c} - v_{in}}{v_{rated} - v_{in}} & v_{in} \le v_{n,c} \le v_{rated} \\ \eta T_{n,c} + k & \text{else} \end{cases} \tag{C.5}$$

$$REcf_{n,solar,c} = \frac{G_{n,c}}{G_{STC}} \cdot [1 + \alpha(T_{n,c} + (u \cdot G_{n,c}) - T_{STC})] \tag{C.6}$$

In Eq. (C.5), the cut-in speed v_{in}, cut-out speed v_{out}, and rated speed v_{rated} are set to 3 m/s, 25 m/s, and 13 m/s, respectively. In Eq. (C.6), the solar radiation under standard test conditions (STC) is $G_{STC} = 1000$ W/m^2,

Table C.2: Structural parameters of the optimized load forecasting model.

Layer	Type	Units	Activation	Function/Notes
Input Layer	Input	(24, D)	-	D denotes the feature dimension.
1st LSTM Layer	LSTM	128	Tanh	Learns primary patterns.
Dropout	Dropout	-	-	Rate = 0.3.
2nd LSTM Layer	LSTM	64	Tanh	Extracts high-level features.
Dropout	Dropout	-	-	Rate = 0.2.
FC Layer 1	Dense	128	ReLU	Feature transformation.
Dropout	Dropout	-	-	Rate = 0.1.
FC Layer 2	Dense	64	ReLU	Dimensionality reduction.
Output Layer	Dense	1	Linear	Scaled load forecast value.

and the standard temperature $T_{STC} = 25°\text{C}$. The wind speed at the hub height of 80 m (v_{80m}) is derived using the power law equation:

$$v_{80m} = v_{10m}\left(\frac{80m}{10m}\right)^{\beta} \tag{C.7}$$

where β is the wind shear exponent derived from local terrain roughness.

Appendix D. Mathematical Formulation of Benders Decomposition and Algorithm

As introduced in Section 3.3, the minimax regret optimization is decoupled into a Master Problem (MP) and a Subproblem (SP).

The MP seeks the optimal investment vector X and introduces an auxiliary variable θ to approximate the maximum regret across scenarios. Its mathematical formulation is as follows:

$$\begin{aligned} &\min \theta \\ \text{s.t.}\quad &\theta \geq C_{total,s}(X) - B_s^* = \sum_{p\in P} w_p(C_{inv,p}(X_p) + Q_{s,p}(X_{s,p})) - B_s^*, \quad \forall s \in \Omega \\ &X_p \in \chi \end{aligned} \tag{D.1}$$

For each scenario s, we enforce the constraint $X_{s,p} = \bar{X}_p$ and denote its dual multiplier by $\pi_{s,p,i}$, thereby deriving the corresponding Benders optimality cut:

$$\theta \geq \sum_{p\in P}\left(w_p(C_{inv,p}(\bar{X}_p) + Q_{s,p}(\bar{X}_p)) + \sum_{i\in I}\pi_{s,p,i}(x_{p,i} - \bar{x}_{p,i})\right) - B_s^*, \quad \forall s \in \Omega \tag{D.2}$$

Given the capacity investment plan $\bar{X}_p$ determined by the MP, the algorithm proceeds to the SP phase. For each scenario $s \in \Omega$, the SWITCH model performs economic dispatch optimization independently to compute the

total system cost over the entire planning horizon. The SP formulation is:

$$\begin{aligned} & \min(C_{inv,s,p}(X_{s,p}) + Q_{s,p}(X_{s,p})) \\ \text{s.t.} \quad & X_{s,p} = \bar{X}_p \\ & X_{s,p} \in \chi \end{aligned} \tag{D.3}$$

Algorithm 1: Benders Decomposition for MMR Model

Input: Scenario set Ω, Perfect information baselines $\{B_s^*\}$, Unit investment costs $\{c_i\}$, Capacity limits X^{max}, Tolerance ϵ

Output: Optimal investment decision $X^* = \{x_i^* \mid i \in \mathcal{I}\}$

$k \leftarrow 0$; $LB^{(k)} \leftarrow -\infty$; $UB^{(k)} \leftarrow +\infty$; $\mathcal{C} \leftarrow \emptyset$;

Initialize first-stage decision $X^{(k)} \leftarrow \frac{1}{|\Omega|} \sum_{s\in\Omega} X_s^*$ (where X_s^* is the optimal capacity for scenario s);

while *Optimality Gap* $(UB - LB)/UB > \epsilon$ **do**

  Execute **SWITCH** simulations for all scenarios $s \in \Omega$ given fixed $X^{(k)}$;

  foreach *scenario* $s \in \Omega$ **do**

    Extract minimized system operational cost $Q_s(X^{(k)})$;

    Extract dual variables $\pi_{s,i}^{(k)}$ associated with capacity constraints for each resource $i \in \mathcal{I}$;

    Calculate scenario-specific regret: $R_s^{(k)} \leftarrow \sum_{i\in\mathcal{I}} c_i x_i^{(k)} + Q_s(X^{(k)}) - B_s^*$;

  end

  $UB \leftarrow \min\left(UB, \max_{s\in\Omega} R_s^{(k)}\right)$;

  foreach *scenario* $s \in \Omega$ **do**

    $\hat{Q}_s^{(k)}(X) \leftarrow Q_s(X^{(k)}) + \sum_{i\in\mathcal{I}} \pi_{s,i}^{(k)}(x_i - x_i^{(k)})$;

    Generate Regret Cut: $\theta \geq \sum_{i\in\mathcal{I}} c_i x_i + \hat{Q}_s^{(k)}(X) - B_s^*$;

    Update the constraint set: $\mathcal{C} \leftarrow \mathcal{C} \cup \{\text{Regret Cut}_s\}$;

  end

  Solve MP using LP solver (CPLEX) in Python:

    min θ

    s.t. $X \in \chi$ (where $\chi = \{0 \leq x_i \leq X_i^{max}, \sum \varepsilon \cdot x_i \leq E_{carbon}^{limit}\}$)

      θ and X subject to all constraints in $\mathcal{C}$;

  $X^{(k+1)} \leftarrow X_{optimal\_from\_MP}$;

  $LB \leftarrow \theta_{optimal\_from\_MP}$;

  $k \leftarrow k + 1$;

end

return $X^* \leftarrow X^{(k)}$;

Algorithm 1 executes the bi-level decoupling iterative process. Convergence is guaranteed by the boundedness of the decision space $\mathcal{X}$ and the linearity of the operational dispatch subproblems. By pre-computing the scenario-specific benchmark costs B_s^*, the algorithm transforms robustness requirements into dynamically generated linear constraints. At each iteration, it updates the lower and upper bounds (LB and UB) of the regret value. Once

the gap closes to within a vanishingly small tolerance, the resulting decision X^* is identified as the optimal initial investment scenario, offering maximal risk-hedging capability over the uncertainty set Ω.

Appendix E. Detailed Data Assumptions and Physical Correction Logic

Appendix E.1. Renewable Energy and Thermal Power Parameters

The simulation of renewable energy generation relies on high-fidelity meteorological datasets. Specifically, the original wind speed data at a 10-meter height is extrapolated to a typical hub height of 80 meters using the standard wind shear model. The maximum developable capacity is constrained by regional land-use data, estimated based on conservative power density assumptions: 1.5 MW/km^2 for onshore wind and 35 MW/km^2 for utility-scale solar PV. Coal fuel costs are modeled exogenously, referencing thermal coal spot prices in the neighboring Datong region, adjusted for calorific value, and standardized to USD/MMBtu.

Appendix E.2. Physical Correction Mechanism for Load Forecasting

While the deep learning model trained with MSE effectively preserves the temporal structure of the load profile, the distributional characteristics inherent in historical training data often hinder the model's ability to fully capture the risks of nonlinear load surges driven by future extreme heatwaves and cold spells. To mitigate the limitations of purely data-driven approaches, this study incorporates a physical correction mechanism based on standard temperature sensitivity analysis methods used in power systems. By integrating Lvliang's local central heating policies and climatic characteristics, we calibrated the load response model specifically for extreme temperature intervals.

Specifically, asymmetric thresholds for temperature-sensitive load response are established. For summer cooling demand, referring to the definition of thermal comfort zones in Chinese cities ($18 \sim 24$°C) by Yang et al. (Yang et al., 2024) and the national standard Meteorological Conditions Grades for Power Demand (GB/T 40242-2021), we set 26°C as the cooling activation threshold. This setting reflects that, against the backdrop of significantly increased air conditioning penetration (Chen et al., 2021), once the air temperature breaches this critical point, minor temperature fluctuations rapidly translate into significant peak pressure on the power grid. Regarding winter heating demand, considering Lvliang as a typical heating region in Northern China, the system relies primarily on coal/gas-fired central heating within the $5 \sim 18$°C range, where electricity load exhibits strong inelastic characteristics (Asadoorian et al., 2008); consequently, 5°C is set as the supplementary electric heating threshold, meaning significant electric auxiliary heating responses are triggered only when temperatures drop below this level (Fan et al., 2019).

Based on these thresholds, the model introduces piecewise linear correction coefficients: load demand increases by 3% for every 1°C rise in summer temperature, and by 1% for every 1°C drop in winter temperature. Here, the higher summer coefficient aligns with the high sensitivity of urban-scale power loads to extreme heat (Chen et al., 2021; Zheng et al., 2020); conversely, the lower winter coefficient objectively reflects the "coal-dominated, electricity-supplemented" heating energy structure in Northern China, where the response intensity to Heating Degree Days (HDD) is significantly lower than that to Cooling Degree Days (CDD) (Fan et al., 2019). Comparative

analysis with actual historical operation data demonstrates that the load curves calibrated via this mechanism exhibit evolutionary trends highly consistent with real-world data during extreme weather days, validating the physical effectiveness of this correction method.

This paper generates and compares the time-series curves of temperature, load demand, and renewable energy resource potential under three typical climate states: TDY, EWY, and ECY.

Appendix F. Convergence Analysis of the Benders Decomposition Algorithm

This appendix presents the iterative convergence profile of the MMR model solved using the Benders decomposition algorithm, as detailed in Appendix D. The convergence criterion is set to an optimality gap of $\mathcal{E} = 0.01\%$. The convergence is demonstrated by the evolution of the Lower Bound (LB) and Upper Bound (UB) of the maximum regret value across iterations. As shown in Fig. F, the gap between LB and UB systematically reduces, achieving convergence to the optimal solution within 30 iterations, confirming the computational efficiency and stability of the adopted solution strategy.

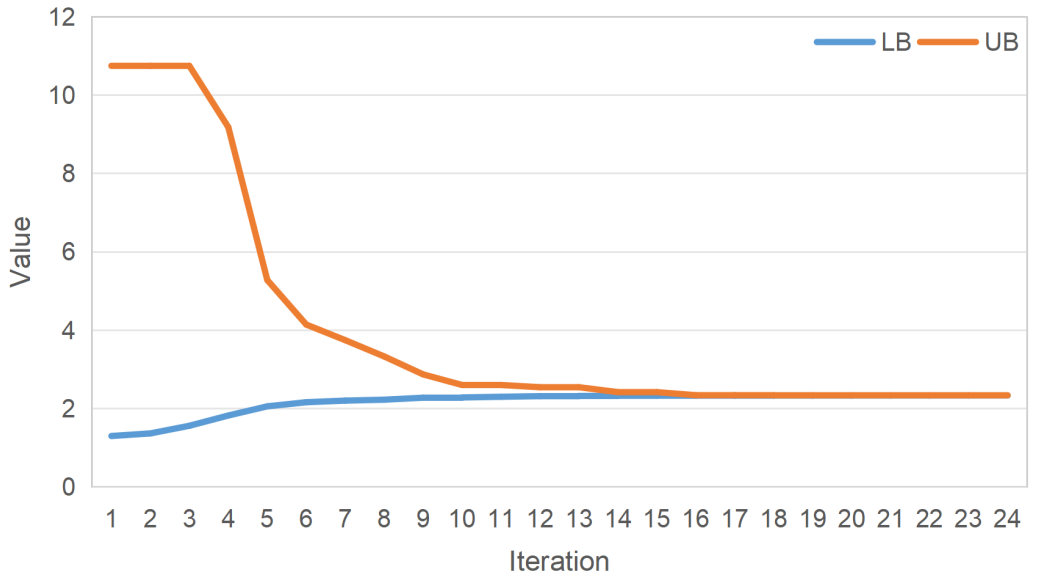

Figure F: Iterative Convergence Curve of MMR Model

Appendix G. Comparison of Cumulative Installed Capacity Expansion between MMR and Representative Deterministic Baselines

This appendix provides the complete set of cumulative installed capacity expansion diagrams for all 27 Deterministic (DET) planning pathways, supplementing the representative baselines shown in Fig. 7 of Section 4.3. These results visually demonstrate the severe path dependence inherent in deterministic planning, where the initial capacity configuration significantly varies based on the assumed climate state (ECY, TDY, or EWY) at the first decision node (2030).

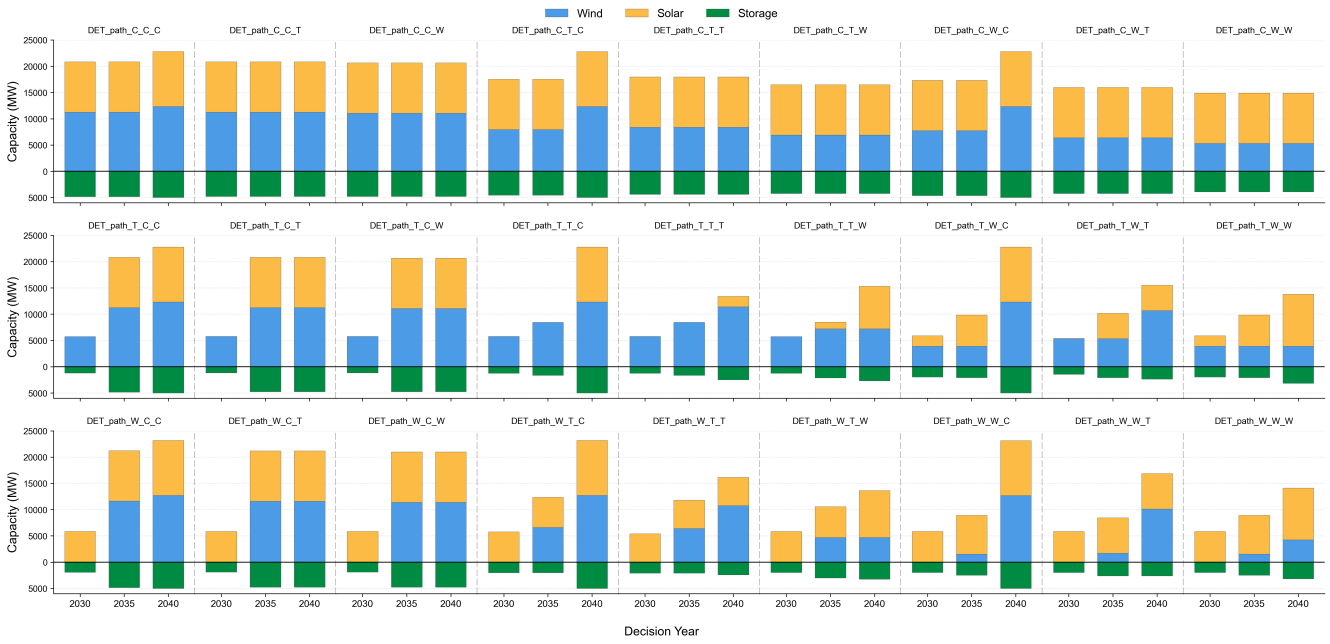

Figure G: Cumulative Installed Capacity Expansion for All 27 Deterministic Pathways

Appendix H. Detailed Reliability Evaluation of Deterministic Benchmarks

The detailed performance evaluation of the MMR scenario against all 27 DET benchmark solutions across the full scenario set is presented here. As shown in Fig. H, the MMR scenario strictly constrains maximum risk exposure to the lowest possible level. In contrast, the vast majority of DET scenarios exhibit significantly elevated maximum UER with peaks exceeding 13%, reflecting the risk of resilience collapse in deterministic planning when encountering non-designed pathways. While certain DET scenarios derived from grim scenarios avoid extreme UER peaks through highly specialized initial capacity configurations, they often incur substantial regret costs in typical or warm climate realizations. This underscores the strategic advantage of the MMR scenario in simultaneously striking an optimal balance between physical reliability and economic efficiency.

Appendix I. Comprehensive Scenario-Wise Performance Evaluation Scatter Plots

This appendix provides the complete set of cost-reliability trade-off scatter plots, comparing the MMR solution against all 27 individual Deterministic (DET) planning baselines across all climate pathways. These plots serve to supplement the three representative comparisons presented in Fig. 8. The visualization demonstrates the consistent superiority and optimal hedging strategy of the MMR scenario across the entire uncertainty space, even when compared individually against specialized DET solutions.

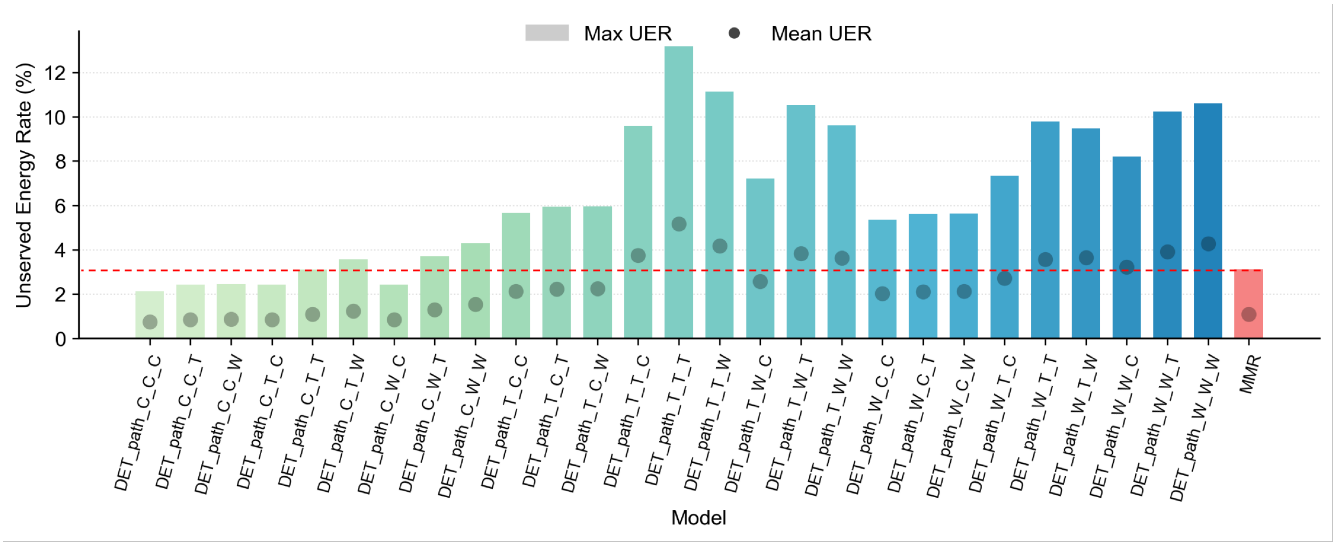

Figure H: Maximum and mean Unserved Electricity Rate (UER) comparison diagram between MMR and DET models.

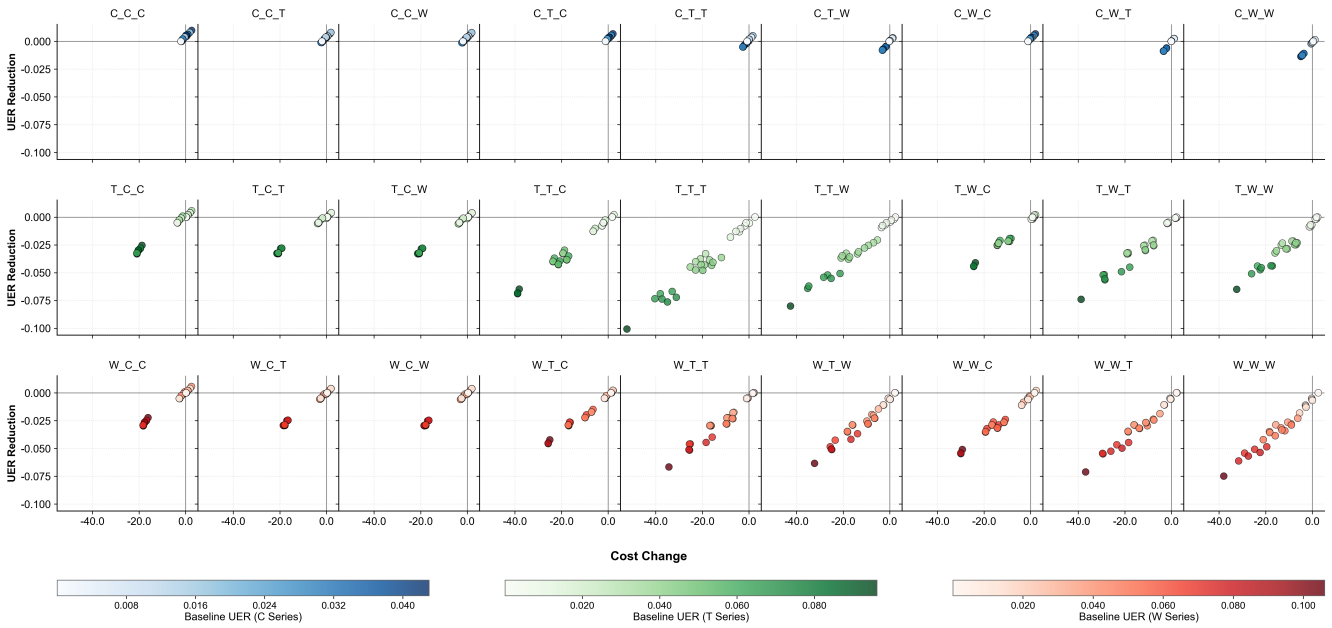

Figure I: Cost-Reliability Trade-off for MMR vs. All Deterministic Paths